This is the accepted manuscript made available via CHORUS. The article has been published as:

Imaging Hidden Objects with Spatial Speckle Intensity Correlations over Object Position

Jason A. Newman, Qiaoen Luo, and Kevin J. Webb

Phys. Rev. Lett. **116**, 073902 — Published 18 February 2016

DOI: 10.1103/PhysRevLett.116.073902

Imaging Hidden Objects with Spatial Speckle Intensity Correlations over Object Position

Jason A. Newman, Qiaoen Luo, and Kevin J. Webb*

School of Electrical and Computer Engineering, Purdue University

465 Northwestern Ave, West Lafayette, IN 47907 USA

Abstract

We present a coherent optical method for wavelength-resolution imaging of moving objects hidden within thick randomly scattering media. Spatial speckle intensity correlations as a function of object position are shown to provide access to the spatially-dependent dielectric constant of the moving object. This speckle correlation imaging method yields field-based information previously inaccessible in heavily scattering environments. Proof of concept experimental results show excellent agreement with the theory. This new imaging approach will be valuable in high resolution imaging in tissue and other scattering environments where natural motion occurs or the object position can be controlled.

PACS numbers: 42.25.Dd, 41.20.Jb, 05.40.-a 42.30.Ms

* Corresponding author: webb@purdue.edu

The ability to image through scattering media with light has garnered immense interest throughout the last several years [1–7]. However, randomly scattering inhomogeneities in the imaging environment interact with the object of interest and the illumination source and, with sufficient scatter, can completely obscure the object [8]. We provide a new method to coherently image a moving object hidden in heavily scattering media.

The memory effect permits imaging through thin randomly scattering media [3, 9, 10]. Also, using wavefront control, it has been possible to focus through a scattering domain [6], hinting at the future promise with, for instance, ultrasonic guide stars [11]. Wavefront control has been combined with the memory effect to image through thin scattering media [3, 12, 13]. Also, measurement of the transmission matrix for the random medium provides information that can allow for imaging through random scatter [14], but this requires suitable characterization data.

A number of localization methods has been developed. For example, with a stationary point scatterer of interest in a background of moving scatters, the average intensity transmission can yield the position of the stationary scatterer, and transverse localization information exists in the average of the difference of speckle patterns (with and without the stationary scatterer) [15]. Localization can also be accomplished in a diffusion framework, with weakly interacting scatterers, [16, 17]. Control of the coherence in speckle pattern difference images can reveal the presence of hidden inhomogeneities [18].

Sophisticated imaging methods have been developed for diffuse optical tomography to achieve geometrical features roughly defined by the transport length, l^* [19, 20]. Greater accuracy can be achieved with high energy photons, where ballistic information (that allows back-projection, for instance) provides tracking data in X-ray phase contrast imaging [21] with use of geometrical optics [22]. However, beyond the physics related to multiply scattering light, use of visible infrared light can be desirable to allow various forms of spectroscopy, and for cost, safety and technology reasons.

The aforementioned and related prior work leads to the position that imaging with wavelength scale resolution in multiply scattering media has been limited to the degree of scatter where wavefront control (with a guide star) or the memory effect can be applied. We show a means to achieve high resolution optical images with multiply scattered coherent light through essentially arbitrarily thick scattering media, limited only by signal-to-noise requirements at the detector, when speckle images are captured as a function of object

position.

We demonstrate a method for imaging moving objects embedded within thick, randomly scattering media that applies provided there is enough scatter to have randomized fields that are zero-mean circular Gaussian [23]. In this scattering regime, our method is not limited by the thickness of the scattering medium, making it complementary to existing speckle imaging approaches [24]. The approach, illustrated in Fig. 1(a), provides a description of the spatial speckle intensity correlation as a function of object position for a moving object hidden inside of a scattering medium, and allows for the moving hidden object to be imaged. We describe the environment as a static random scattering medium with an embedded object at some position inside the random medium. However, in reality, the randomly scattering medium only needs to be static during a particular span of time. We define the normalized intensity for polarized light exiting a random medium as $\tilde{I} = (I - \langle I \rangle)/\sigma_I$, where $\langle I \rangle$ is the mean intensity and σ_I is the standard deviation of the intensity. The speckle contrast ratio [8], $\sigma_I/\langle I \rangle$, is unity for polarized coherent light and fully developed speckle statistics. In this case, the intensity statistics are negative exponential and the underlying field statistics, assuming weakly interacting scatterers, are zero-mean circular Gaussian, a property of the field statistics that we will use.

We write the spatial speckle intensity correlation as $\langle \tilde{I}(\mathbf{r}; \mathbf{r}_o)\tilde{I}(\mathbf{r}; \mathbf{r}_o + \Delta\mathbf{r}_o)\rangle$, where $\tilde{I}(\mathbf{r}; \mathbf{r}_o)$ is the normalized intensity at position $\mathbf{r}$ with an object embedded inside the random scattering medium at a reference position described by $\mathbf{r}_o$, and the object's movement is described by $\Delta\mathbf{r}_o$. Assuming zero-mean circular Gaussian statistics, we can express the normalized intensity correlation in terms of the normalized field correlation using a moment theorem as [25]

$$\langle \tilde{I}(\mathbf{r}; \mathbf{r}_o)\tilde{I}(\mathbf{r}; \mathbf{r}_o + \Delta\mathbf{r}_o)\rangle = \left|\langle \tilde{E}(\mathbf{r}; \mathbf{r}_o)\tilde{E}^*(\mathbf{r}; \mathbf{r}_o + \Delta\mathbf{r}_o)\rangle\right|^2, \tag{1}$$

where $\tilde{E} = E/\sigma_E$ is the normalized scalar field and σ_E is the standard deviation of the field. With zero-mean circular Gaussian fields, $\sigma_E = \langle |E|^2 \rangle^{1/2} = \langle I \rangle^{1/2} = \sqrt{\sigma_I}$ [25, 26].

In developing an expression for the imaging problem, we use a scalar wave equation to describe the interaction of the speckled optical field with the object of interest (that is being translated). This corresponds to the physical optics approximation, so that the vector field problem associated with the moving scatterer can be treated by the scalar wave equation. This treatment can be generalized for an arbitrary sized object through use of the vector

wave equation.

We write the total field, $E(\mathbf{r};\mathbf{r}_o)$, as

$$E(\mathbf{r};\mathbf{r}_o) = E_i(\mathbf{r}) + E_s(\mathbf{r};\mathbf{r}_o), \tag{2}$$

where $E_i(\mathbf{r})$ is the field in the scattering medium without the object and $E_s(\mathbf{r};\mathbf{r}_o)$ is the field scattered by the object. The wave equation for the electric field, assuming constant permeability, can be written as

$$\nabla^2 \left[E_i(\mathbf{r}) + E_s(\mathbf{r};\mathbf{r}_o)\right] + k_0^2\epsilon_i(\mathbf{r}) \left[E_i(\mathbf{r}) + E_s(\mathbf{r};\mathbf{r}_o)\right] + k_0^2\epsilon_s(\mathbf{r};\mathbf{r}_o) \left[E_i(\mathbf{r}) + E_s(\mathbf{r};\mathbf{r}_o)\right] = 0, \tag{3}$$

where $k_0^2 = (2\pi/\lambda_0)^2$, λ_0 is the free-space wavelength, $\epsilon_i(\mathbf{r})$ is the spatially-dependent dielectric constant of the random medium, and $\epsilon_s(\mathbf{r};\mathbf{r}_o)$ is the difference with and without the embedded object centered at $\mathbf{r}_o$. Knowing that $\nabla^2 E_i(\mathbf{r}) + k_0^2\epsilon_i(\mathbf{r})E_i(\mathbf{r}) = 0$, moving all of the terms containing $\epsilon_s(\mathbf{r};\mathbf{r}_o)$ to the right hand side, and using (2), we write (3) as

$$\nabla^2 E_s(\mathbf{r};\mathbf{r}_o) + k_0^2\epsilon_i(\mathbf{r})E_s(\mathbf{r};\mathbf{r}_o) = -k_0^2\epsilon_s(\mathbf{r};\mathbf{r}_o)E(\mathbf{r};\mathbf{r}_o). \tag{4}$$

Using the Green's function solution to (4), $G(\mathbf{r}',\mathbf{r};\mathbf{r}_o)$, we write the scattered field as

$$E_s(\mathbf{r};\mathbf{r}_o) = \int \mathrm{d}\mathbf{r}' E(\mathbf{r}';\mathbf{r}_o)k_0^2\epsilon_s(\mathbf{r}';\mathbf{r}_o)G(\mathbf{r}',\mathbf{r};\mathbf{r}_o). \tag{5}$$

With (5), the total field at some point, $\mathbf{r}$, becomes

$$E(\mathbf{r};\mathbf{r}_o) = E_i(\mathbf{r}) + k_0^2 \int \mathrm{d}\mathbf{r}' E(\mathbf{r}';\mathbf{r}_o)\epsilon_s(\mathbf{r}';\mathbf{r}_o)G(\mathbf{r}',\mathbf{r};\mathbf{r}_o). \tag{6}$$

We use (6) to write the electric field correlation over object position, at detector position $\mathbf{r}_d$, as

$$\begin{aligned}\langle E(\mathbf{r}_d;\mathbf{r}_o)E^*(\mathbf{r}_d;\mathbf{r}_o+\Delta\mathbf{r}_o)\rangle = \Bigg\langle &\left[E_i(\mathbf{r}_d) + k_0^2\int \mathrm{d}\mathbf{r}' E(\mathbf{r}';\mathbf{r}_o)\epsilon_s(\mathbf{r}';\mathbf{r}_o)G(\mathbf{r}',\mathbf{r}_d;\mathbf{r}_o)\right] \\ &\times \left[E_i^*(\mathbf{r}_d) + k_0^2\int \mathrm{d}\mathbf{r}'' E^*(\mathbf{r}'';\mathbf{r}_o+\Delta\mathbf{r}_o)\epsilon_s^*(\mathbf{r}''+\Delta\mathbf{r}_o;\mathbf{r}_o+\Delta\mathbf{r}_o)G^*(\mathbf{r}'',\mathbf{r}_d;\mathbf{r}_o+\Delta\mathbf{r}_o)\right]\Bigg\rangle.\end{aligned} \tag{7}$$

At this point, we recognize the statistical independence of the various terms in (7), such as the field without the scattering object and the scattered field, and use this to separate the averaging. In addition, the final term of the expansion of (7) is reduced to a single

integral using the assumption that the contributions to the correlation occur only over the joint support [27], giving

$$\begin{aligned}\langle E(\mathbf{r}_d;\mathbf{r}_o)E^*(\mathbf{r}_d;\mathbf{r}_o+\Delta\mathbf{r}_o)\rangle &= \langle|E_i(\mathbf{r}_d)|^2\rangle \\ &+ k_0^2\langle E_i(\mathbf{r}_d)\rangle\langle\int \mathrm{d}\mathbf{r}'' E^*(\mathbf{r}'';\mathbf{r}_o+\Delta\mathbf{r}_o)\epsilon_s^*(\mathbf{r}''+\Delta\mathbf{r}_o;\mathbf{r}_o+\Delta\mathbf{r}_o)G^*(\mathbf{r}'',\mathbf{r}_d;\mathbf{r}_o+\Delta\mathbf{r}_o)\rangle \\ &+ k_0^2\langle E_i^*(\mathbf{r}_d)\rangle\langle\int \mathrm{d}\mathbf{r}' E(\mathbf{r}';\mathbf{r}_o)\epsilon_s(\mathbf{r}';\mathbf{r}_o)G(\mathbf{r}',\mathbf{r}_d;\mathbf{r}_o)\rangle \\ &+ k_0^4\int \mathrm{d}\mathbf{r}'\langle E(\mathbf{r}';\mathbf{r}_o)E^*(\mathbf{r}';\mathbf{r}_o+\mathbf{r}_o)G(\mathbf{r}',\mathbf{r}_d;\mathbf{r}_o)G^*(\mathbf{r}',\mathbf{r}_d;\mathbf{r}_o+\Delta\mathbf{r}_o)\rangle \\ &\quad\times\epsilon_s(\mathbf{r}';\mathbf{r}_o)\epsilon_s^*(\mathbf{r}'+\Delta\mathbf{r}_o;\mathbf{r}_o+\Delta\mathbf{r}_o). \end{aligned} \tag{8}$$

The second and third terms in (8) are zero because $\langle E_i(\mathbf{r}_d)\rangle$ has zero mean. These observations allow us to write (8) as

$$\begin{aligned}\langle E(\mathbf{r}_d;\mathbf{r}_o)E^*(\mathbf{r}_d;\mathbf{r}_o+\Delta\mathbf{r}_o)\rangle &= \langle|E_i(\mathbf{r}_d)|^2\rangle \\ &+ k_0^4\int \mathrm{d}\mathbf{r}'\langle E(\mathbf{r}';\mathbf{r}_o)E^*(\mathbf{r}';\mathbf{r}_o+\Delta\mathbf{r}_o)G(\mathbf{r}',\mathbf{r}_d;\mathbf{r}_o)G^*(\mathbf{r}',\mathbf{r}_d;\mathbf{r}_o+\Delta\mathbf{r}_o)\rangle \\ &\quad\times\epsilon_s(\mathbf{r}';\mathbf{r}_o)\epsilon_s^*(\mathbf{r}'+\Delta\mathbf{r}_o;\mathbf{r}_o+\Delta\mathbf{r}_o). \end{aligned} \tag{9}$$

With sufficient scatter, the average of the field and Green's function in the last term in (9) can be reduced to a slowly varying function of space, C, leading to

$$\langle E(\mathbf{r}_d;\mathbf{r}_o)E^*(\mathbf{r}_d;\mathbf{r}_o+\Delta\mathbf{r}_o)\rangle = \langle|E_i(\mathbf{r}_d)|^2\rangle + C\int \mathrm{d}\mathbf{r}'\epsilon_s(\mathbf{r}';\mathbf{r}_o)\epsilon_s^*(\mathbf{r}'+\Delta\mathbf{r}_o;\mathbf{r}_o+\Delta\mathbf{r}_o), \tag{10}$$

with

$$C = \langle E(\mathbf{r}';\mathbf{r}_o)E^*(\mathbf{r}';\mathbf{r}_o+\Delta\mathbf{r}_o)G(\mathbf{r}',\mathbf{r}_d;\mathbf{r}_o)G^*(\mathbf{r}',\mathbf{r}_d;\mathbf{r}_o+\Delta\mathbf{r}_o)\rangle. \tag{11}$$

With C in (10) constant, the statistics are stationary over object position, such that the field mean and variance are independent of embedded object position, $\mathbf{r}_o$. The field variance at the detector, $\sigma_E^2 = \langle|E|^2\rangle$, with E from (6), becomes

$$\sigma_E^2 = \left\langle\left|E_i(\mathbf{r}_d) + k_0^2\int \mathrm{d}\mathbf{r}' E(\mathbf{r}';\mathbf{r}_o)\epsilon_s(\mathbf{r}';\mathbf{r}_o)G(\mathbf{r}',\mathbf{r}_d;\mathbf{r}_o)\right|^2\right\rangle. \tag{12}$$

Expansion of the terms in (12) leads to

$$\begin{aligned}\sigma_E^2 =&\langle |E_i(\mathbf{r}_d)|^2\rangle \\ &+ k_0^2\langle E_i(\mathbf{r}_d)\rangle\langle \int \mathrm{d}\mathbf{r}' E^*(\mathbf{r}';\mathbf{r}_o)\epsilon_s^*(\mathbf{r}';\mathbf{r}_o)G^*(\mathbf{r}',\mathbf{r}_d;\mathbf{r}_o)\rangle \\ &+ k_0^2\langle E_i^*(\mathbf{r}_d)\rangle\langle \int \mathrm{d}\mathbf{r}' E(\mathbf{r}';\mathbf{r}_o)\epsilon_s(\mathbf{r}';\mathbf{r}_o)G(\mathbf{r}',\mathbf{r}_d;\mathbf{r}_o)\rangle \\ &+ k_0^4\langle \int \mathrm{d}\mathbf{r}' E(\mathbf{r}';\mathbf{r}_o)\epsilon_s(\mathbf{r}';\mathbf{r}_o)G(\mathbf{r}',\mathbf{r}_d;\mathbf{r}_o)\int \mathrm{d}\mathbf{r}'' E^*(\mathbf{r}'';\mathbf{r}_o)\epsilon_s^*(\mathbf{r}'';\mathbf{r}_o)G^*(\mathbf{r}'',\mathbf{r}_d;\mathbf{r}_o)\rangle. \quad (13)\end{aligned}$$

Using the same joint support argument that was used to arrive at (9), recognizing that the middle two terms in (13) are zero, due to $\langle E_i(\mathbf{r}_d)\rangle$ having zero mean, and again treating the average over the field and Green's function to be slowly varying, (13) is reduced to

$$\sigma_E^2 =\langle |E_i(\mathbf{r}_d)|^2\rangle + C\int \mathrm{d}\mathbf{r}' \left|\epsilon_s(\mathbf{r}';\mathbf{r}_o)\right|^2. \quad (14)$$

The normalized electric field autocorrelation, at detector position $\mathbf{r}_d$, is written as

$$\langle \tilde{E}(\mathbf{r}_d;\mathbf{r}_o)\tilde{E}^*(\mathbf{r}_d;\mathbf{r}_o+\Delta\mathbf{r}_o)\rangle =\frac{1}{\sigma_E^2}\langle E(\mathbf{r}_d;\mathbf{r}_o)E^*(\mathbf{r}_d;\mathbf{r}_o+\Delta\mathbf{r}_o)\rangle. \quad (15)$$

We use (9) and (14) in (15) to obtain an expression for the normalized electric field spatial correlation in terms of the object's autocorrelation as

$$\langle \tilde{E}(\mathbf{r}_d;\mathbf{r}_o)\tilde{E}^*(\mathbf{r}_d;\mathbf{r}_o+\Delta\mathbf{r}_o)\rangle = \frac{\langle |E_i(\mathbf{r}_d)|^2\rangle + C\int \mathrm{d}\mathbf{r}'\epsilon_s(\mathbf{r}';\mathbf{r}_o)\epsilon_s^*(\mathbf{r}'+\Delta\mathbf{r}_o;\mathbf{r}_o+\Delta\mathbf{r}_o)}{\langle |E_i(\mathbf{r}_d)|^2\rangle + C\int \mathrm{d}\mathbf{r}' \left|\epsilon_s(\mathbf{r}';\mathbf{r}_o)\right|^2}. \quad (16)$$

Equation (16) shows that information about the object is available in the measured speckle intensity correlation, obtained from (15) using a moment theorem [25]. In the case of no embedded moving object, the second terms in both the numerator and the denominator of (16) are zero, leaving us with, as expected, a constant correlation of 1. The mean intensity without the object gives $\langle |E_i(\mathbf{r}_d)|^2\rangle$, and this can be obtained using a model or a prior measurement without the object. The unknowns in (16) are then two constants, C, as given in (11) and constant because of the heavy scatter in relation to the object motion, and $\int \mathrm{d}\mathbf{r}' \left|\epsilon_s(\mathbf{r}';\mathbf{r}_o)\right|^2$, and the autocorrelation of the object's spatially dependent dielectric constant. With sufficient measurement data, the two constants and the object (defined by its dielectric constant) can in principle be determined. We consider a special case to simplify and demonstrate the result in (16).

With a strongly interacting moving embedded object, the second terms in the numerator and denominator in (16) will be much larger than the first term. The resulting complete decorrelation of the speckle image therefore occurs when the difference in dielectric constant of the object and the background, ϵ_s, is significant. When the second term is sufficiently large, (16) can be reduced to

$$\langle \tilde{E}(\mathbf{r}_d;\mathbf{r}_o)\tilde{E}^*(\mathbf{r}_d;\mathbf{r}_o+\Delta\mathbf{r}_o)\rangle \approx \frac{\int \mathrm{d}\mathbf{r}'\epsilon_s(\mathbf{r}';\mathbf{r}_o)\epsilon_s^*(\mathbf{r}'+\Delta\mathbf{r}_o;\mathbf{r}_o+\Delta\mathbf{r}_o)}{\int \mathrm{d}\mathbf{r}'\left|\epsilon_s(\mathbf{r}';\mathbf{r}_o)\right|^2}. \tag{17}$$

We use (17) in (1) to write the normalized intensity correlation in terms of the field correlation as

$$\langle \tilde{I}(\mathbf{r}_d;\mathbf{r}_o)\tilde{I}(\mathbf{r}_d;\mathbf{r}_o+\Delta\mathbf{r}_o)\rangle \approx \frac{\left|\int \mathrm{d}\mathbf{r}'\epsilon_s(\mathbf{r}';\mathbf{r}_o)\epsilon_s^*(\mathbf{r}'+\Delta\mathbf{r}_o;\mathbf{r}_o+\Delta\mathbf{r}_o)\right|^2}{\left|\int \mathrm{d}\mathbf{r}'\left|\epsilon_s(\mathbf{r}';\mathbf{r}_o)\right|^2\right|^2}. \tag{18}$$

Equation (18) describes the spatial speckle correlation in terms of the normalized autocorrelation of an embedded moving object, where the object is described in terms of its dielectric constant. The averaging can be assumed to be over the scatterer configuration or, due to the statistical independence of the speckle spots, over detectors at different points, such as pixels in a CCD camera. The use of a CCD camera allows a very large number of independent measurements to be made simultaneously while the embedded object moves.

An inversion of (18) allows for the imaging of moving objects hidden within scattering media in terms of the object's optical properties. We emphasize that the resolution of the image is then about one wavelength, dictated by use of propagating waves. This inversion requires a phase retrieval to determine ϵ_s from its correlation. This phase retrieval could be achieved through various means, such as an iterative phase retrieval where known constraints are applied in the real and Fourier domains [28] or even through the use of the bispectral phase obtained from a third-order correlation over space as a dual variable application of previous frequency correlations [29, 30].

Equation (18) was experimentally verified for a special case using the setup shown in Fig. 1(b). An 850 nm laser diode with a linewidth less than 10 MHz illuminated a 3 mm thick slab placed between the laser source and the object and a 9 mm thick randomly scattering slab was placed between the camera and the object of interest. The two slabs were separated by 3.5 cm. Both slabs, clear acrylic with embedded 50 nm diameter TiO_2 particles, had a reduced scattering coefficient, an inverse measure of the mean free path, of 4 cm^{-1}. A 4-f spatial filter and magnifying lens were used to control the size of the speckle pattern imaged

by a CCD camera. The object of interest was a circular hole in an absorbing sheet. The hole was moved in the plane between the scattering slabs and speckle images were taken as a function of position. The imaging arrangement resulted in a spot about 1 mm in diameter on the back of the scattering medium being imaged to the camera, and the heavy scatter resulted in the measured mean intensity being independent of scan position. These speckle images were then used to calculate the spatial speckle intensity correlation as a function of object position. The data from each of the 480,000 pixels were averaged to form an estimate of the spatial speckle correlation. The experimental results for 500 μm and 1000 μm diameter circular apertures along with the expected correlation using (18) (assuming that $\epsilon_s(\mathbf{r};\mathbf{r}_o)$ was zero at the hole and large and imaginary everywhere else) are shown in Fig. 2(a). Excellent agreement between the experimental results and theory is shown, forming a strong basis for the validity of (18). Note that $l^* = 2.5$ mm for this scattering medium and that the distance scale in Fig. 2(a) makes it clear the accuracy of the inverted image is very high relative to l^* and should be on the order of the optical wavelength. We used measured speckle images and reconstructed an image for the hidden 500 μm diameter aperture with the model described in (18), and obtained the result shown in Fig. 2(b). Because the discrete sampling of the correlation was quite coarse in the experiment, we selected zero crossings from simulated data in the reconstruction. The Fourier domain data was filtered using a 2D Hamming window before the final inverse Fourier transform to arrive at the spatial image shown.

We investigated a set of square cylindrical scattering rods, 8 mm on each side, that were scanned between the same two scattering slabs (3 mm thick on the source side and 9 mm on the detector side, referring to Fig. 1(b), with $\mu_s' = 4$ cm^{-1}), with camera intensity images captured at each scan position. One rod had the same scattering properties as the slabs, one had a larger reduced scattering coefficient of $\mu_s' = 14$ cm^{-1}, and the other was an absorbing black rod. The rods were moved a total distance of 5 mm and speckle images were taken every 40 μm. An additional twenty images were taken at 0.1 μm steps. The normalized intensity correlations were calculated from the measured data and the results are shown in Figs. 3(a) and (b). The long range correlations in Figure 3(a) go to zero at 8 mm, corresponding to the moving object's size. The short range results in Figure 3(b) decorrelate on the far-subwavelength scale. This rapid decrease is due to edge movement, and the differences in the correlations are associated with the microstructure in the rods. The black rod effectively lets no light pass, so its rough surface movement is the primary contributor to

the small decrease, while the $\mu_s' = 14$ cm^{-1} and $\mu_s' = 4$ cm^{-1} rods are increasingly more transmissive, leading to a more significant wavelength-scale decorrelation due to the embedded scatterers. On both length scales, the scatter from the object dictates the decorrelation rate. These correlations are independent of the scattering background because the scatter is heavy enough that the mean intensity measured is independent of object motion over the range used in these experiments. Despite each rod having the same physical dimensions, the spatial speckle correlations are clearly different. This allows us to not only determine that there is an object moving between the slabs, but also to identify the object. For example, these correlations could be used in the classification and identification of objects moving through naturally occurring scattering environments such as tissue, clouds, or other cluttered background. A library of object correlations could be assembled which would allow for the rapid identification of objects without requiring computationally expensive inversions.

In the imaging method we have described based on the inversion of (18) with measured intensity data as a function of object position, the movement of the object does not necessarily have to be controlled and can be due to natural motion. The effective step size would then be determined by the object's velocity and image acquisition time. If the object's motion is not known, then an analogous problem can be described where, assuming that the object is known, the object's motion can be determined and tracked. The speckle intensity correlation can be rewritten in terms of the object's time dependent velocity, $\mathbf{v}(t)$ and time, t, where $\mathbf{r} = \mathbf{r}_0 + \Delta\mathbf{r} = \mathbf{r}_0 + \int_{t_0}^{t_1} \mathbf{v}(t)dt$. This allows for sensing and tracking of hidden objects. Alternatively, if the object's velocity is considered uniform over a time-frame of interest, the resulting correlation could be used to identify the object. We should note that such information related to correlations over object position is distinct from the temporal correlations related to diffusing-wave spectroscopy [31], where a large number of scatterers are producing the decorrelation.

We have presented a theory that allows for imaging (through the inversion of the spatial speckle correlation) moving objects embedded within scattering media at wavelength resolution. This allows for new sensing and imaging opportunities at wavelengths and in scattering regimes that were previously inaccessible. The use of speckle images and various types of correlations, such as the spatial correlations presented here alongside frequency and temporal correlations [3–5, 30, 32], comprise a powerful set of tools for the analysis of scattering environments and the ability to sense, track, and image in scattering environments.

In tissue, blood cells or contrast agents in vessels could move quickly relative to surrounding tissue that dominates the scatter, conforming to the arrangement assumed. Another relevant situation is a moving object under sea ice or snow, with both the light source and detector above. The work should also impact imaging in various aerosols. Our method applies across a broad range of the electromagnetic spectrum and even for other field-based imaging methods where there is vulnerability to random scatter. All of these applications require methods that can compensate for the subject of interest being embedded inside of a thick scattering environment.

This work was supported by the National Science Foundation (NSF) under grants 1028610 and 1218909.

---

[1] D. S. Wiersma, Nature Photon. **7**, 188 (2013).

[2] B. Redding, M. A. Choma, and H. Cao, Nature Photon. **6**, 355 (2012).

[3] J. Bertolotti, E. G. van Putten, C. Blum, A. Lagendijk, W. Vos, and A. P. Mosk, Nature **491**, 232 (2012).

[4] S. Popoff, G. Lerosey, M. Fink, A. C. Boccara, and S. Gigan, Nat. Commun. **1**, 81 (2010).

[5] O. Katz, E. Small, Y. Bromberg, and Y. Silberberg, Nature Photon. **5**, 372 (2011).

[6] I. M. Vellekoop and A. P. Mosk, Opt. Lett. **32**, 2309 (2007).

[7] J. A. Newman and K. J. Webb, Phys. Rev. Lett. **113**, 263903 (2014).

[8] J. W. Goodman, *Speckle Phenomena in Optics: Theory and Applications* (Roberts and Company Publishers, 2007).

[9] I. Freund, M. Rosenbluh, and S. Feng, Phys. Rev. Lett. **61**, 2328 (1988).

[10] I. Freund, Physica A **168**, 49 (1990).

[11] B. Judkewitz, Y. M. Wang, R. Horstmeyer, A. Mathy, and C. Yang, Nature Photon. **7**, 300 (2013).

[12] O. Katz, E. Small, and Y. Silberberg, Nature Photon. **6**, 549 (2012).

[13] O. Katz, P. Heidmann, M. Fink, and S. Gigan, Nature Photon. **8**, 784 (2014).

[14] S. M. Popoff, , A. Aubry, G. Lerosey, M. Fink, A. C. Boccara, and S. Gigan, Phys. Rev. Lett. **107**, 263901 (2011).

[15] R. Berkovits and S. Feng, Phys. Rev. Lett. **65**, 3120 (1990).

[16] P. N. den Outer, T. M. Nieuwenhuizen, and A. Lagendijk, J. Opt. Soc. Am. A **10**, 1209 (1993).

[17] G. Cao, V. Gaind, C. A. Bouman, and K. J. Webb, Opt. Lett. **32**, 3026 (2007).

[18] J. D. McKinney, M. A. Webster, K. J. Webb, and A. M. Weiner, Opt. Lett. **25**, 4 (2000).

[19] S. R. Arridge and M. Schweiger, Proc. of Information Processing in Medical Imaging (1993).

[20] A. B. Milstein, S. Oh, K. J. Webb, C. A. Bouman, Q. Zhang, D. A. Boas, and R. P. Millane, Appl. Opt. **42**, 3081 (2003).

[21] K. A. Nugent, T. E. Gureyev, D. F. Cookson, D. Paganin, and Z. Barnea, Phys. Rev. Lett. **77**, 2961 (1996).

[22] K. S. Morgan, D. M. Paganin, and K. K. W. Siu, Appl. Phys. Lett. **100**, 124102 (2012).

[23] J. W. Goodman, *Statistical Optics* (New York, Wiley-Interscience, 1985).

[24] S. Feng, C. Kane, P. A. Lee, and A. D. Stone, Phys. Rev. Lett. **61**, 834 (1988).

[25] I. S. Reed, IRE Trans. Inform. Theory **8**, 194 (1962).

[26] A. Papoulis and S. U. Pillai, *Probability, Random Variables, and Stochastic Processes* (McGraw-Hill, 2002).

[27] J. A. Newman and K. J. Webb, Opt. Lett. **37**, 1136 (2012).

[28] J. R. Fienup, J. Opt. Soc. Am. A **4**, 118 (1987).

[29] A. W. Lohmann and B. Wirnitzer, Proc. of the IEEE **72**, 889 (1984).

[30] M. A. Webster, K. J. Webb, and A. M. Weiner, Phys. Rev. Lett. **88**, 033901 (2002).

[31] D. J. Pine, D. A. Weitz, P. M. Chaikin, and E. Herbolzheimer, Phys. Rev. Lett. **60**, 1134 (1988).

[32] Z. Wang, M. A. Webster, A. M. Weiner, and K. J. Webb, J. Opt. Soc. Am. A **23**, 3045 (2006).

FIGURES

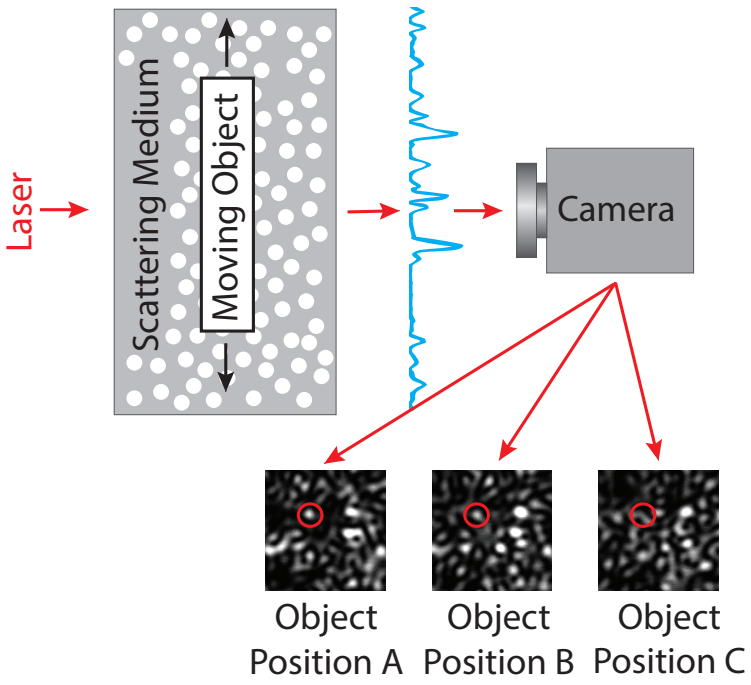

(a)

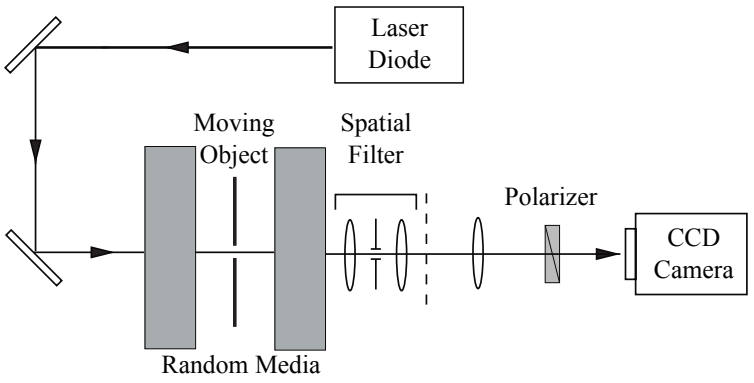

(b)

FIG. 1. (a) Conceptual for imaging a moving object hidden within a scattering medium by collecting speckle intensity images as a function of object position. (b) Experiment with an 850 nm laser illuminating a pair of scattering slabs. An object was placed between the slabs and scanned using a set of linear stages. Speckle images were collected at each object position using a 4-f spatial filter, magnifying optics, and a polarizer.

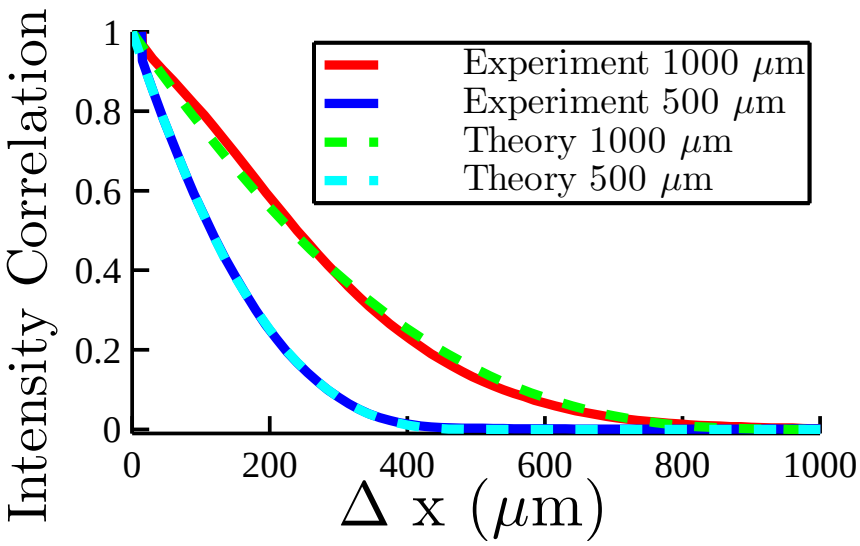

(a)

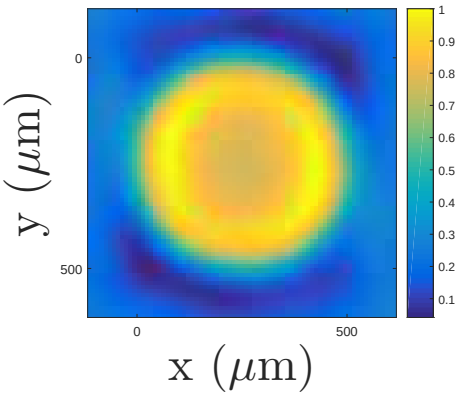

(b)

FIG. 2. (a) Spatial speckle intensity correlation for a 1000 μm and a 500 μm diameter circular aperture placed between two scattering slabs, a 3 mm thick slab between the laser and aperture and a 9 mm thick slabs between the aperture and camera, with $\mu_s' = 4$ cm^{-1}. Our theoretical result for the correlation, (18), matches very well to the experimental results. (b) Reconstructed image of the hidden 500 μm circular aperture using the experimental intensity correlation data over object position.